# Dynamics and Control of a Tethered Enhanced Gravity Tractor Performing Asteroid Deflection

Haijun Shen,* Carlos M. Roithmayr,† and Yingyong Li‡

The dynamics and control of an Enhanced Gravity Tractor (EGT) augmented with a tether for deflecting an asteroid are studied. A conventional EGT consists of collected asteroidal mass collocated with the spacecraft. Because of the presence of a tether, the collected mass is placed where the EGT would have been without a tether, and the spacecraft is placed farther away from the asteroid. Doing so improves the fuel efficiency and safety margin of the EGT operation without significantly sacrificing the gravitational attraction between the asteroid and the EGT. The tether is modeled as a series of particles connected by spring-dashpot systems. Physical properties of the tether are selected to be similar to those of the SPECTRA-1000, Kevlar-29, and Kevlar-49 fibers. It is assumed that control is applied only to the spacecraft, and there is no active control associated with the collected mass. A Proportional-Derivative (PD) controller is employed to maintain the spacecraft and the collected mass at desired positions relative to the asteroid. Numerical simulations of tethered EGT operations at 2008 EV5, Itokawa, Apophis, and a fictitious ellipsoidal asteroid are performed. It is demonstrated that a PD controller is capable of accomplishing the control objectives. The gravity gradient and the control force keep the tether stretched throughout a normal tethered EGT operation, and the load on the tether is well within the design limit of the tether material. While including multiple particles in the tether model is essential in capturing details of tether vibration, the number of particles does not significantly affect the motions of the collected mass and the spacecraft. In addition, the distance from the asteroid mass center to the collected mass should be chosen judiciously in the case of a rotating slender asteroid; some distance ranges should be avoided as excessive lateral oscillations can be excited by resonance between the asteroid rotation and tether pendular motion.

## I.  Introduction

Collisions between objects that make up our solar system are commonplace, as evidenced by numerous craters on planets, moons, asteroids, and comets. In fact, it is theorized in Refs. [1–3] that most of the boulders and regolith on asteroids such as 21 Lutetia, 433 Eros, etc., are formed by such collisions. The planet Earth is not immune from the danger. Even though our atmosphere protects the Earth by incinerating objects with diameters of 10 m or less before they reach the surface, larger objects can survive the atmospheric transit and cause catastrophic damage.

The threat is real, and the best conceivable mitigation consists of detecting and deflecting potentially hazardous objects. Various ways of deflecting an asteroid have been proposed. High-energy schemes utilizing kinetic impactors (Refs. [4–6]) and nuclear or non-nuclear blasts (Ref. [7]) are capable of achieving large deflection in a short period of time, which is effective if a threat is detected with a short warning time. These schemes are not suitable for rubble-pile asteroids held together by weak gravity and cohesion. For smaller asteroids with a long warning time, a few low-energy schemes have been proposed. In Ref. [8], Bombardelli and Pelaez suggest blasting an asteroid surface with ion beams, which transfers momentum from the ion particles to the asteroid.

Mechanical attachment of a propulsion system to an asteroid is problematic. First, it may be difficult to obtain firm attachment if the asteroid is a rubble pile or composed of low-strength material. Second, an asteroid's rotational motion interferes with the application of thrust in the best direction for deflection. These problems are avoided with a concept proposed by Lu and Love in Ref. [9]; it involves no physical contact and is known as the Gravity Tractor (GT). A spacecraft is placed so that it leads the asteroid in its heliocentric trajectory. Two thrusters impart momentum to the spacecraft, which tugs the asteroid through mutual gravitational attraction. The thrusters are canted (angled) in order

---
*Supervising engineer, Analytical Mechanics Associates, Inc., Hampton, VA 23666. shen@ama-inc.com
†Senior aerospace engineer, Vehicle Analysis Branch, NASA Langley Research Center, Hampton, VA 23681. carlos.m.roithmayr@nasa.gov
‡Aerospace engineer, Structural and Thermal Systems Branch, NASA Langley Research Center, Hampton, VA 23681. yingyong.li@nasa.gov

to prevent impingement of the plume streams on the asteroid surface. However, the portion of thrust that contributes to effective asteroid deflection is proportional to the cosine of the cant angle; wasted thrust is proportional to the sine of the cant angle. The disadvantage of thruster cant is addressed by McInnes in Ref. [10] by placing the spacecraft in a halo orbit in front of the asteroid. A properly sized halo orbit makes it possible to prevent plume impingement without canting the thrusters. This idea is extended by Wie in Ref. [11] to include multiple spacecraft in a halo orbit to expedite deflection. Another innovation introduced in Ref. [11] is the addition of a solar sail to the gravity tractor. The sail is oriented so as to provide a component of Solar Radiation Pressure (SRP) force in the direction of the asteroid's motion and impart momentum to the asteroid-spacecraft system. In Ref. [12], Carroll suggests using a solar sail in combination with ballast collected from the asteroid and suspended from the gravity tractor with a tether. The gravity tractor is made more effective by adding mass to the spacecraft because doing so increases the gravitational attraction between the asteroid and the spacecraft. Collecting boulders and regolith from the asteroid surface is an attractive way of adding mass to the spacecraft.

Use of a boulder to demonstrate asteroid deflection was proposed as part of the Asteroid Redirect Mission as discussed in Refs. [13] and [14], where the spacecraft with augmented mass is referred to as an Enhanced Gravity Tractor (EGT). In-situ utilization of native asteroidal material reduces the launch cost and trip time compared to sending the same amount of mass from Earth. Compared to regular GT operations without the additional mass, the EGT requires less time to achieve the same amount of deflection. Reference [14] shows that the deflection times can be reduced by a factor of 10 to 50 or more with the EGT, depending on the propulsion system's capability and the amount of mass collected.

In a previous paper, Ref. [15], we explored the use of a tether and a solar sail to make an EGT more effective and provide operational simplification. A container of asteroidal material is attached to a tether and placed close to the asteroid to increase gravitational attraction, while the spacecraft is placed farther away from the asteroid for a better margin of safety. In the case of a single EGT placed in front of the asteroid, as in Ref. [9], the increased distance afforded by a tether permits a smaller thruster cant angle. Operationally, the halo orbit employed in Ref. [10] requires tight orbit control. Instead of using a halo orbit to provide lateral displacement of the spacecraft, we employ a solar sail. In the case of a single spacecraft placed in the asteroid's heliocentric orbit plane and slightly farther away from the sun than the asteroid, as in Ref. [11], the cant angle of the towing thrusters can be eliminated. The solar sail can be oriented so that it provides only the lateral displacement, or so that it also provides some of the towing force. Two additional spacecraft with solar sails can be placed to either side of the asteroid's heliocentric orbit plane; in this case, their solar sails can be oriented so as to maintain the out-of-plane positions. The efficiency of these new concepts has been analyzed with respect to the asteroid size, tether length, collected mass, and distance from the collected mass to the asteroid, with the assumption that the asteroids of interest are spherical in shape, and tether dynamics has been neglected.

In the present paper we take a closer look at the concept of a single EGT that employs a tether to suspend the collected mass in front of the asteroid. The aim is to understand the dynamical behavior of the spacecraft, the collected mass, and the tether during gravity tractor operations. The tether is modeled as a series of particles connected by spring-dashpot systems. Through simulations we show that 1) a Proportional-Derivative (PD) controller is sufficient to keep the spacecraft at a desired position; 2) the control force and gravity gradient between the collected mass and the spacecraft is able to keep the tether taut throughout the EGT operation, and the load on the tether is within the design limit of the tether material; 3) including multiple particles in the tether model is essential to capture details of tether vibration, but is not essential in characterizing the motions of the collected mass and the spacecraft; 4) the desired position for the collected mass cannot be chosen arbitrarily because, at some positions, resonance between the asteroid rotation and pendular motion can excite excessive lateral displacement of the collected mass, which is especially significant for irregularly shaped and slow-spinning asteroids.

## II.    System Model

### A.    Tethered EGT

Figure 1 shows two in-track EGTs side by side. On the left, the EGT and collected mass are collocated, whereas they are separated by a tether in the image on the right. It is apparent that for in-track EGTs it is necessary to cant the thrusters in order to prevent the thrusters from pluming the asteroid surface. Excessive thruster canting can make the asteroid deflection inefficient in terms of propellant consumption as a significant component of the thrust vector is in essence wasted instead of contributing to deflecting the asteroid. Thus, it is desirable to minimize the cant angle. Moving the collocated EGT away from the asteroid reduces the thruster cant angle, but it also reduces the gravitational
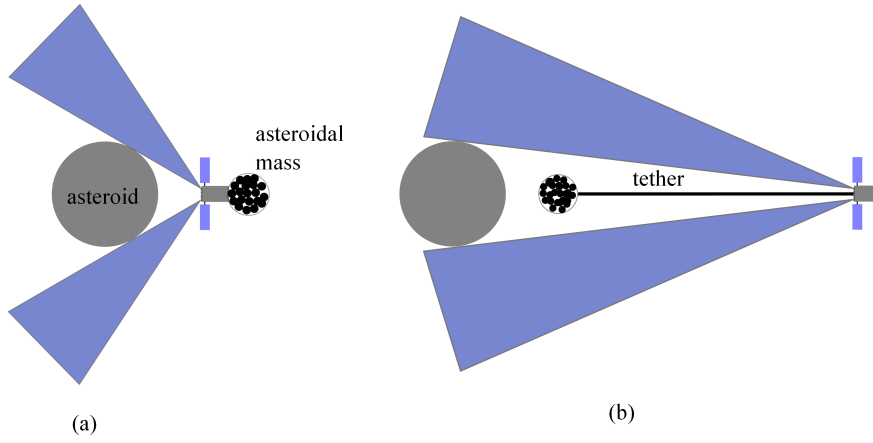
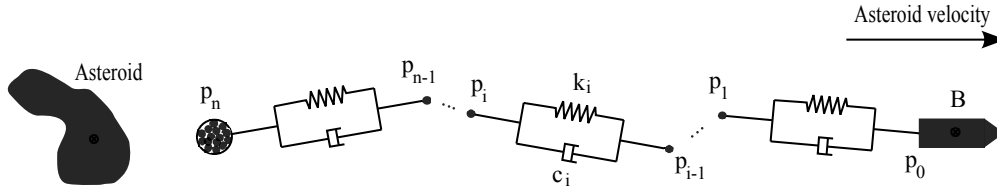Figure 1: In-track EGT: (a) without a tether; (b) with a tether.



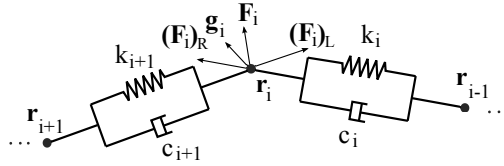Figure 2: Spring-mass-damper model of the tethered EGT.



Figure 3: Forces acting on a generic particle of the tether.

attraction, which diminishes the effectiveness of the EGT in deflecting the asteroid. To overcome this dilemma, we propose utilizing a tether to separate the collected mass and the spacecraft, which in turn permits a reduction in the thruster cant angle; EGT effectiveness is preserved as long as the collected mass is significantly more massive than the spacecraft. As illustrated in Fig. 1(b), by furnishing the EGT with a tether, the collected asteroidal mass can be placed where the EGT would have been without the tether, and the spacecraft can be moved further away from the asteroid. Doing so improves the thrusting efficiency by reducing the thruster cant angle and simultaneously increases the safety margin for the spacecraft.

The spacecraft and the collected asteroidal mass are on the two ends of the tether. The spacecraft is modeled as a rigid body $B$, and the collected mass is treated as a single particle. The tether is considered to be an untapered flexible cable with uniform density. It is modeled as a number of particles connected by idealized linear springs and dampers. Each particle has three degrees of freedom relative to the spacecraft. This model is illustrated in Fig. 2. The tether is divided into $n$ segments: $p_0$ denotes the point at which the tether is attached to the spacecraft, $p_i$ $(i = 1, \ldots, n-1)$ are the particles belonging to the tether, and $p_n$ is the collected mass. $k_i$ and $c_i$ $(i = 1, \ldots, n)$ are the spring constant and damping coefficient of the $i^{\text{th}}$ spring-damper system.

A number of materials with high specific strength have been considered for tethered spacecraft missions, such as SPECTRA-1000 used in SEDS-1 and SEDS-2 (Small Expendable Deployer System) missions and Kevlar 29 in the Atmospheric Tether Mission (Ref. [16]). In this paper, the baseline physical properties of the tether are selected to be similar to those of the SPECTRA-1000 (Ref. [17]), Kevlar-29, and Kevlar-49 fibers (Ref. [18]). Specifically, the density and Young's modulus of the tether are chosen to be 1440 kg/m$^3$, and 100 GPa, respectively. The spring constant of the tether varies linearly with the length of the tether. For a 1-km tether with a diameter of 3 mm, the spring constant is 706.9 N/m, and the mass of the tether is merely 10 kg.

The objective of employing the EGT is to pull the asteroid in the direction of its heliocentric velocity vector, which is the most effective way of applying thrust for deflection as pointed out in Ref. [19]. To describe motion of the EGT, we introduce a reference frame $L$ in which the asteroid's mass center is fixed, and define unit vectors fixed in $L$ as follows. $\hat{\mathbf{x}}_L$ has the same direction as the asteroid's heliocentric velocity, $\hat{\mathbf{y}}_L$ is directed opposite to the angular momentum vector of the asteroid orbit, and $\hat{\mathbf{z}}_L$ completes the right-handed vector basis. For intervals of time that are small in comparison to the asteroid's heliocentric orbit period, $L$ can be regarded as an inertial reference frame. A second set of right-handed unit vectors is defined to be fixed in spacecraft body $B$. $\hat{\mathbf{x}}_B$ is parallel to the longitudinal axis of the spacecraft and directed toward the nose. $\hat{\mathbf{y}}_B$ and $\hat{\mathbf{z}}_B$ are orthogonal to each other, and span the plane perpendicular to $\hat{\mathbf{x}}_B$. It is assumed that the position vector from the tether attachment point $p_0$ to the spacecraft center of mass has the same direction as $\hat{\mathbf{x}}_B$.

The masses of the spacecraft and tether particles are denoted by $m_B$ and $m_i$ $(i = 1, \ldots, n)$, respectively. The position vectors from the asteroid mass center to the spacecraft mass center, the tether attachment point on the spacecraft, and the particles are represented by $\mathbf{r}_B$, $\mathbf{r}_0$, and $\mathbf{r}_i$ $(i = 1, \ldots, n)$, respectively, and the velocities in $L$ of these points are denoted by $\mathbf{v}_B$, $\mathbf{v}_0$, and $\mathbf{v}_i$ $(i = 1, \ldots, n)$, respectively. Figure 3 shows the forces acting on $p_i$. The gravitational force exerted by the asteroid is $\mathbf{g}_i$. The force exerted on $p_i$ by the $i^{\text{th}}$ spring-damper system is $(\mathbf{F}_i)_R$, whereas that applied by the $(i+1)^{\text{th}}$ system is $(\mathbf{F}_i)_L$. $\mathbf{F}_i$ is the resultant force acting on $p_i$,

$$\mathbf{F}_i = \mathbf{g}_i + (\mathbf{F}_i)_R + (\mathbf{F}_i)_L \qquad (i = 1, \ldots, n) \tag{1}$$

where $(\mathbf{F}_n)_L = \mathbf{0}$. In view of the flexibility of the tether material and the large ratio of tether length to diameter, it is assumed that the tether does not resist any deformation except when it is stretched, and the resisting force is parallel to the unit position vector $\hat{\mathbf{P}}^i_{i-1}$ from $p_{i-1}$ to $p_i$,

$$\hat{\mathbf{P}}^i_{i-1} = \frac{\mathbf{r}_i - \mathbf{r}_{i-1}}{|\mathbf{r}_i - \mathbf{r}_{i-1}|} \qquad (i = 1, \ldots, n) \tag{2}$$

Thus, for the $i^{\text{th}}$ particle, the force $(\mathbf{F}_i)_R$ due to the $i^{\text{th}}$ spring-damper system is given by

$$(\mathbf{F}_i)_R = \begin{cases} \left[ -k_i(d^i_{i-1} - L_i) - c_i(\mathbf{v}_i - \mathbf{v}_{i-1}) \cdot \hat{\mathbf{P}}^i_{i-1} \right] \hat{\mathbf{P}}^i_{i-1} & \text{if } d^i_{i-1} > L_i \\ \mathbf{0} & \text{if } d^i_{i-1} \leq L_i \end{cases} \qquad (i = 1, \ldots, n) \tag{3}$$

where $d^i_{i-1} = |\mathbf{r}_i - \mathbf{r}_{i-1}|$ is the distance between the particles $p_{i-1}$ and $p_i$, and $L_i$ is the unstretched length of the $i^{\text{th}}$ tether segment.

## B.  Gravitational Field Models

An asteroid's gravitational potential can be modeled with a spherical harmonic series in the region outside a circumscribing sphere, where convergence of the series is guaranteed. In the region between the asteroid's surface and the circumscribing sphere, a polyhedral gravity model based on the assumption of constant density can be used, as discussed in Ref. [20]. Polyhedron shape models for a number of asteroids are publicly available; for example, see Ref. [21]. For a constant-density polyhedron, one can obtain spherical harmonic coefficients to arbitrary degree and order from the shape models, using the method set forth in Ref. [22]. Prior to commencing gravity tractor operations, the spacecraft will be used to characterize the size, shape, boulder and regolith distribution, spin state, and gravity field of the asteroid. It is assumed that characterization of the asteroid yields spherical harmonic coefficients up to the third degree and order with 1% accuracy, $3\sigma$. Monte Carlo simulations indicate that 1%-$3\sigma$ random errors in the spherical harmonic coefficients cause equivalent 1%-$3\sigma$ errors in the gravitational force. Thus, in this paper, we assume the spacecraft guidance system has knowledge of the $3\times3$ spherical harmonic coefficients, but a 1% error is introduced into the computed gravity force. Four asteroids are studied in this paper, namely 2008 EV5, Itokawa, Apophis, and a fictitious triaxial ellipsoid, for which the true gravitational fields are represented by $8\times8$, $20\times20$, and $20\times20$ spherical harmonics, and a closed-form solution provided in Ref. [23], respectively.

## C.  The Control Law

During gravity tractor operations, it is desired that the collected mass and the spacecraft remain at nominal positions relative to the asteroid mass center, which are located along the $x_L$ axis. Stationkeeping is important: movement away from the asteroid results in reduced gravitational attraction, whereas movement toward the asteroid may result

in a collision. Due to the irregular gravitational field (non-spherical shape) of the asteroid, as the asteroid rotates, the gravitational force per unit mass exerted on the spacecraft and the collected mass at the nominal stationkeeping positions vary. The variation in the gravitational force acts as an external perturbation that affects stationkeeping stability. In addition, an uncontrolled EGT may quickly crash into the asteroid surface due to the mutual gravitational attraction. For example, an uncontrolled EGT placed 350 m, 450 m, and 350 m away from the mass centers of 2008 EV5, Itokawa, and Apophis takes close to 0.7, 1.1, and 0.9 hours, respectively, before it collides with the asteroid surface. Thus, a controller is necessary to keep the collected mass and the spacecraft at their designated positions.

It should be noted that if the spacecraft and collected mass deviate from the nominal positions in the $\hat{\mathbf{y}}_L$-$\hat{\mathbf{z}}_L$ plane (lateral deviations), gravity exerts restoring forces on them so that they have a tendency to return to the nominal positions. In later sections, it will be shown that the lateral deviations are not always stable, but the unstable regions can be avoided by judicious placement of the spacecraft and collected mass. In addition, stable lateral deviations, if not excessive, do not cause appreciable gravity loss in the longitudinal direction and therefore do not diminish the effectiveness of asteroid deflection. Thus, in the paper, we are concerned only with stabilizing the longitudinal deviations from nominal positions along the $x_L$ axis, with the following control force applied on the spacecraft,

$$\mathbf{F}_B = \left\{ \left[ -k_p(\mathbf{r}_B - \mathbf{r}_B^\star) - k_d\mathbf{v}_B - \bar{\mathbf{g}}_B - \sum_{i=1}^{n} \bar{\mathbf{g}}_i \right] \cdot \hat{\mathbf{x}}_L \right\} \hat{\mathbf{x}}_L \tag{4}$$

where $k_p$ and $k_d$ are positive control gains, and $\mathbf{r}_B^\star$ is the desired nominal position vector $\mathbf{r}_B$ from the asteroid mass center to the spacecraft mass center. Because $\mathbf{v}_B$ is the velocity in $L$ (that is, the velocity relative to the asteroid mass center) of the spacecraft mass center, the desired nominal value is $\mathbf{0}$. $\bar{\mathbf{g}}_B$ and $\bar{\mathbf{g}}_i$ are estimates of the gravitational forces $\mathbf{g}_B$ and $\mathbf{g}_i$ exerted by the asteroid on spacecraft $B$ and particle $p_i$ $(i = 1, \ldots, n)$, respectively. The control force is applied only along the $\hat{\mathbf{x}}_L$ direction. In practice, however, the control force vector in Eq. (4) can be represented by a $3 \times 1$ array containing measure numbers for the vector basis $\hat{\mathbf{x}}_B$, $\hat{\mathbf{y}}_B$, $\hat{\mathbf{z}}_B$. For example, the array representing $\mathbf{F}_B$ contains the measure numbers $\mathbf{F}_B \cdot \hat{\mathbf{x}}_B$, $\mathbf{F}_B \cdot \hat{\mathbf{y}}_B$, and $\mathbf{F}_B \cdot \hat{\mathbf{z}}_B$. During tethered EGT operations the spacecraft is subject to $\mathbf{F}_B$ and $\mathbf{g}_B$ applied at the mass center, together with the force applied by the tether at $p_0$ and a corresponding moment about the mass center.

# III.    Tethered EGT at 2008 EV5

Results of a numerical simulation involving deflection of 2008 EV5 with a tethered EGT are presented in this section. This asteroid has diameters of 420 m, 410 m, and 390 m, and performs simple rotational motion with a period of 3.725 hours, with the spin axis having the same direction as $\hat{\mathbf{y}}_L$. With an assumption of the density being 2000 kg/m³, the gravitational parameter for 2008 EV5 is 4.65 m³/s². In Ref. [15] it has been shown that the benefit offered by a tether diminishes when its length is greater than 10 times the asteroid radius. Thus, the length of the tether is chosen to be 2000 m. It is assumed that the tether is already deployed, and the tethered EGT is in normal operation. Initially the tether is at its natural length of 2 km. For the purpose of modeling the dynamics, the tether is divided into 5 equal segments. The collected mass is initially at its nominal position 350 m from the asteroid mass center. The tether attachment point is 2 m from the spacecraft center of mass, away from the nose. Unit vectors $\hat{\mathbf{x}}_B$, $\hat{\mathbf{y}}_B$, and $\hat{\mathbf{z}}_B$ initially have the same directions as $\hat{\mathbf{x}}_L$, $\hat{\mathbf{y}}_L$, and $\hat{\mathbf{z}}_L$, respectively. The collected mass is assumed to be 1000 metric tons, corresponding to a sphere of 10-m diameter with 2000-kg/m³ density, and the spacecraft mass is 9000 kg. In comparison, the mass for the 2000-m tether is merely 20 kg. The spring constant for the 400-m tether segment is $k_i = 1767.1$ N/m; the damping coefficient of the tether is selected to be $c_i = 0.1$ Ns/m; the control gains are selected as $k_p = 0.05$ N/m and $k_d = 0.5$ Ns/m. An $8 \times 8$ spherical harmonic model of the asteroid's gravity field is regarded as the true field. The controller, however, is provided with only a $3 \times 3$ truncated model. Moreover, errors in gravity field estimation are simulated by increasing the values in the truncated model by 1%.

Figure 4 shows the projections in the directions of $\hat{\mathbf{x}}_L$, $\hat{\mathbf{y}}_L$, and $\hat{\mathbf{z}}_L$ of $\mathbf{r}_B$, the position vector from the asteroid mass center to the spacecraft mass center. Longitudinal displacement in the direction of the asteroid's inertial velocity, $\hat{\mathbf{x}}_L$, is controlled to be within 2 m of approximately 2353.5 m. The lateral displacements of the spacecraft in the directions of $\hat{\mathbf{y}}_L$ and $\hat{\mathbf{z}}_L$ are small, approximately 1 m. Projections in the directions of $\hat{\mathbf{x}}_L$, $\hat{\mathbf{y}}_L$, and $\hat{\mathbf{z}}_L$ of $\mathbf{r}_M$, the position vector from the asteroid mass center to the collected asteroidal mass, are plotted in Fig. 5. The longitudinal displacement of the collected mass has a mean of 351.5 m, and oscillates with an amplitude of less than 2 m. The lateral displacements oscillate with an amplitude of less than 3 m. Because the collected mass is much closer to the asteroid than the spacecraft, the former is affected more than the latter by the irregular gravity field of the asteroid. The reason the mean distances of the collected mass and the spacecraft from the asteroid are slightly greater than their
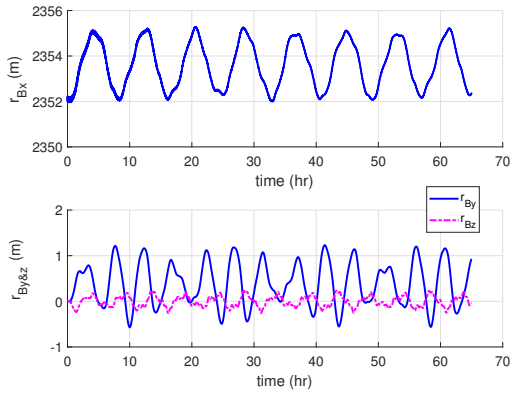
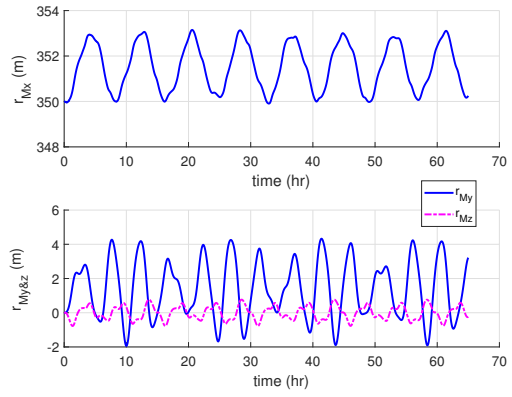Figure 4: Position of the spacecraft mass center projected onto $\hat{\mathbf{x}}_L, \hat{\mathbf{y}}_L, \hat{\mathbf{z}}_L$



Figure 5: Position of the collected asteroidal mass projected onto $\hat{\mathbf{x}}_L, \hat{\mathbf{y}}_L, \hat{\mathbf{z}}_L$
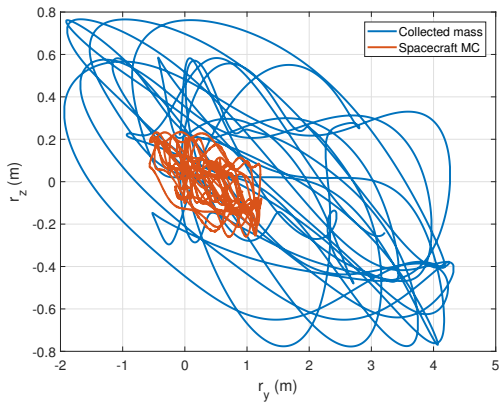


Figure 6: Loci of the collected mass and the spacecraft MC projected in the $\hat{\mathbf{y}}_L$-$\hat{\mathbf{z}}_L$ plane.
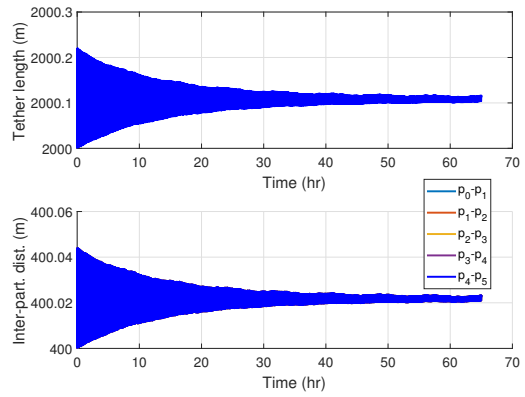


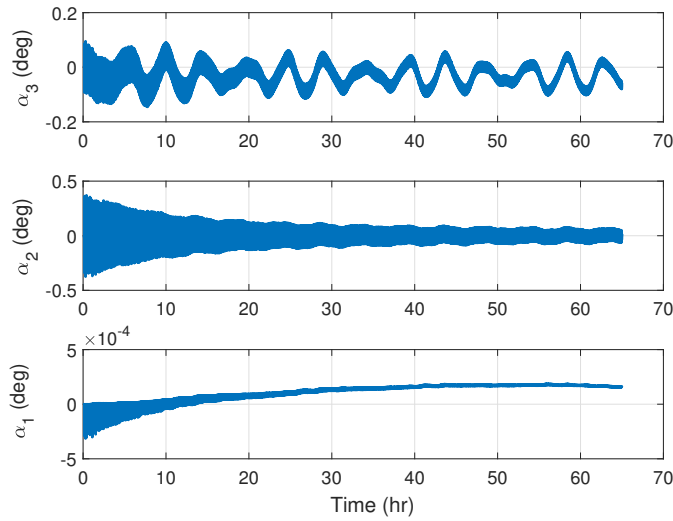Figure 7: Length of the tether and the distances between particles



Figure 8: Attitude of $B$ in $L$, 3-2-1 Euler angles

6

nominal values of 350 m and 2352 m, respectively, is that the gravity has been over-estimated by 1%. It should be noted that the collected mass is not furnished with any thrusters or other effectors that can apply control force.

The 65-hour loci of the collected mass and the spacecraft mass center projected in the $\hat{\mathbf{y}}_L$-$\hat{\mathbf{z}}_L$ plane are shown in Fig. 6. The loci look chaotic, and do not clearly follow any set pattern. The lateral movement along the $\hat{\mathbf{y}}_L$ axis clearly has a bias toward the positive direction. This is caused by the positive component of the gravity vector along the $\hat{\mathbf{y}}_L$ direction at points along $\hat{\mathbf{x}}_L$ axis. The lateral movement in the $\hat{\mathbf{z}}_L$ direction is less than 0.8 m. It will be shown in later sections that the amount of lateral movement does not always remain small for non-spherical and slow spinning asteroids.

The tether length and distances between neighboring particles in the tether model are shown in Fig. 7. It can be seen that the gravity gradient between the collected mass and the spacecraft, along with the control force on the spacecraft, quickly stretches the tether beyond its nominal length of 2000 m. Due to high stiffness of the tether material and the low-gravity environment, the amount of elongation of the tether is small, approximately 10 cm. The tether material considered here can typically sustain elongation of approximately 3% (Refs. [17, 18]) (60 m for the 2000-m tether) before it breaks; therefore, the load on the tether is well within the limit. Similarly, the distances between neighboring particles are slightly greater than the nominal value of 400 m for each tether segment. Throughout the EGT operation, the tether remains taut.

The attitude of the spacecraft relative to frame $L$ can be described with a set of Euler angles $\alpha_3$, $\alpha_2$, $\alpha_1$ associated with a 3-2-1 rotation sequence. Time histories of these angles are presented in Fig. 8. Spacecraft attitude motion is affected only by the force applied by the tether. Given the distance between the spacecraft and the asteroid, as well as the low-gravity environment, the gravitational moment due to the inverse-square term and spherical harmonics is negligible. In addition, no attitude control is applied. It can be seen that the Euler angles remain less than 0.5 deg in absolute value throughout the EGT operation.

# IV.   Number of Particles Composing the Tether

As one having experience with finite element models might expect, increasing the number of particles in the tether model improves the fidelity of the model at the expense of simulation execution time. The effect of the number of particles on the behavior of the collected mass, the spacecraft, the tether, and computer runtime is illustrated in this section. All simulation results discussed in this paper are obtained with MATLAB® R2017a on a laptop computer with Intel® Core™ i7-7820HQ CPU. The stiff solver ode15s in MATLAB is used to integrate the equations of motion.

In the simulations whose results are discussed in this section, a fictitious asteroid is modeled as a triaxial ellipsoid having dimensions $600 \times 400 \times 300$ m (diameter) and a uniform density of 2000 kg/m$^3$. The gravitational parameter for this asteroid is 5.03 m$^3$/s$^2$. The asteroid performs a simple spin about its smallest diameter, with the rotation axis in the same direction as $\hat{\mathbf{y}}_L$. It is assumed that the collected mass is 1000 metric tons, and the spacecraft mass is 9000 kg. The desired location of the collected mass is 600 m from the asteroid mass center. Here the length of the tether is chosen to be 3000 m, which is 10 times the greatest asteroid radius. The initial condition is such that the collected mass is at its desired position, and the tether is at its natural length.

Table 1: Runtime to simulate a 10-hour tethered EGT operation

| Number of particles | 1 | 2 | 3 | 4 | 5 | 8 | 10 |
|---|---|---|---|---|---|---|---|
| Runtime (hr) | 0.068 | 0.87 | 1.6 | 2.3 | 3.6 | 7.4 | 8.5 |

Table 1 shows simulation runtimes for a 10-hour EGT operation and various numbers of particles in the tether model. Note that when the model involves only one particle, its mass is the sum of the masses of the collected asteroidal material and the tether. Conversely, particles that represent tether material have mass of only a few kilograms. The runtime for a single particle is one order of magnitude faster than the case with two particles, and the runtime drastically increases when more particles are included in the tether model. Due to the relatively high stiffness of the tether material, high frequency oscillations are expected for the tether particles. Thus, the time steps for adequately characterizing the dynamics of several particles must be much smaller than the time steps needed in the case of a single particle.

The motion of the tethered EGT system also consists of oscillations with low frequencies, especially those of the collected mass and the spacecraft. Asteroids of diameters between 100 m and 1000 m typically rotate at very slow rates. For example, the rotation periods for the three asteroids examined in the paper, 2008 EV5, Itokawa, and Apophis, are approximately 3.7 hrs, 12.1 hrs, and 263 hrs, respectively, with Apophis also precessing at a period of approximately
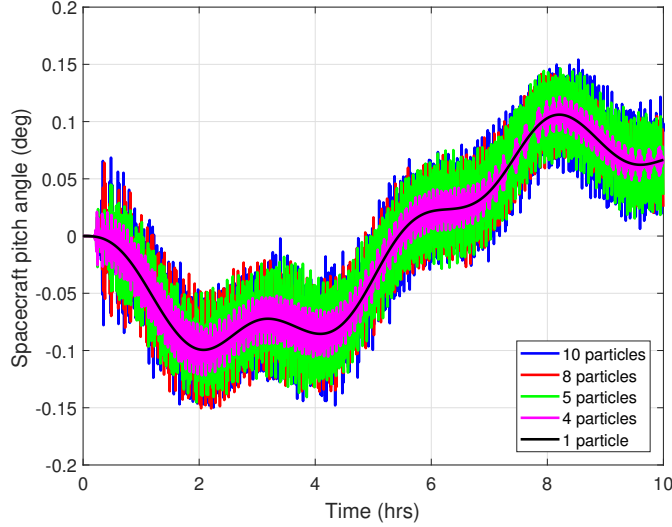
Figure 9: Spacecraft pitch angle profiles resulting from different number of particles in the tether model.

27.4 hrs. Thus, any oscillations of the collected mass and the spacecraft due to asteroid rotations will have long periods. In addition, the gravitational attraction is low in the vicinity of these asteroids, which implies that the lateral oscillations as a result of pendular motion also can have long periods. Therefore, the motions of the collected mass and the spacecraft can only be adequately characterized by simulating long intervals of time, which can be hundreds of hours or more in many cases. However, it is immediately clear from Table 1 that the simulation runtime can quickly become prohibitive if long EGT operations have to be simulated, especially for performing sensitivity analyses where a large number of simulation runs have to be conducted. In what follows, an example is provided to show that the positions and velocities of the collected mass and the spacecraft are not significantly affected by the high frequency vibrations of the tether. Therefore, we assert that mean motions of the collected mass and the spacecraft are adequately characterized with a model having a single particle representing the collected mass.

Profiles of the spacecraft pitch angle obtained with tether models having 1, 4, 5, 8, and 10 particles are shown in Figure 9. Since the asteroid spin axis is parallel to $\hat{\mathbf{y}}_L$, and the asteroid is symmetric about the $\hat{\mathbf{x}}_A$-$\hat{\mathbf{y}}_A$ plane, the motions of the collected mass, spacecraft, and the tether remain in the $\hat{\mathbf{x}}_L$-$\hat{\mathbf{z}}_L$ plane. Thus, spacecraft attitude motion takes place solely in the pitch angle. With only one particle in the tether model collocated with the collected mass, the pitch angle trajectory is a smooth curve. When the number of particles increases, the tether produces high-frequency pitch motion but the mean pitch angle profile remains the same as in the single-particle case. The amplitude of the vibration with 4 particles in the tether model is smaller than the amplitudes associated with 5, 8, and 10 particles. In addition, the vibration amplitude does not increase when more than 5 particles are included in the model. In fact, the standard deviations for the spacecraft pitch angle from the mean profile for the models with 4, 5, 8, and 10 particles are 0.009, 0.025, 0.025, and 0.027 degrees, respectively. Therefore, it is not necessary to use more than 5 particles to characterize the amplitude of the pitch angle vibration. Furthermore, a model having one particle collocated with the collected mass is sufficient to characterize the mean spacecraft pitch angle. It is worth noting that the use of more particles can reveal more modes of tether motion and give one a better picture of actual behavior. However, when planning a tethered EGT mission, the primary interest will be characterizing the stability of the motions of the spacecraft and the collected mass, and the load on the tether, to ensure a safe and smooth operation.

The positions of the spacecraft mass center and the collected mass associated with various numbers of particles in the tether model are shown in Figs. 10 and 11, respectively. In the normal views shown in the left panels, the curves associated with different numbers of particles are hardly distinguishable. More details are revealed when parts of the curves (in black squares on the left panels) are magnified. It can be seen that the position of the spacecraft mass center has longitudinal vibrations of approximately 5-cm amplitude and lateral vibrations approximately several millimeters in amplitude.Figure 11 illustrates that the vibrations on the positions of the collected mass are even weaker. This observation leads us to believe that the positions of the collected mass and the spacecraft mass center are not significantly affected by the tether dynamics, and a tether model with one particle collocated with the collected mass is adequate to capture the mean motions of the spacecraft and the collected mass.
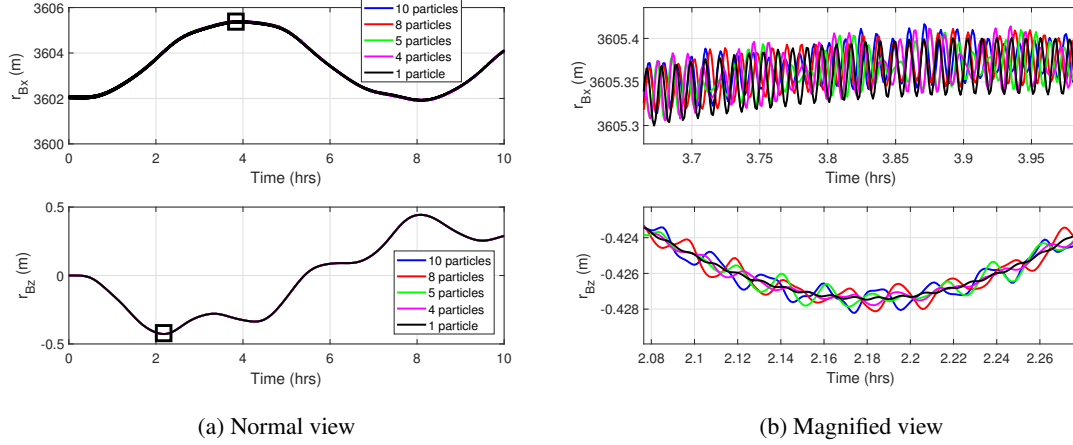
(a) Normal view                    (b) Magnified view

Figure 10: The position profiles of the spacecraft mass center as the number of particles in the tether model varies.



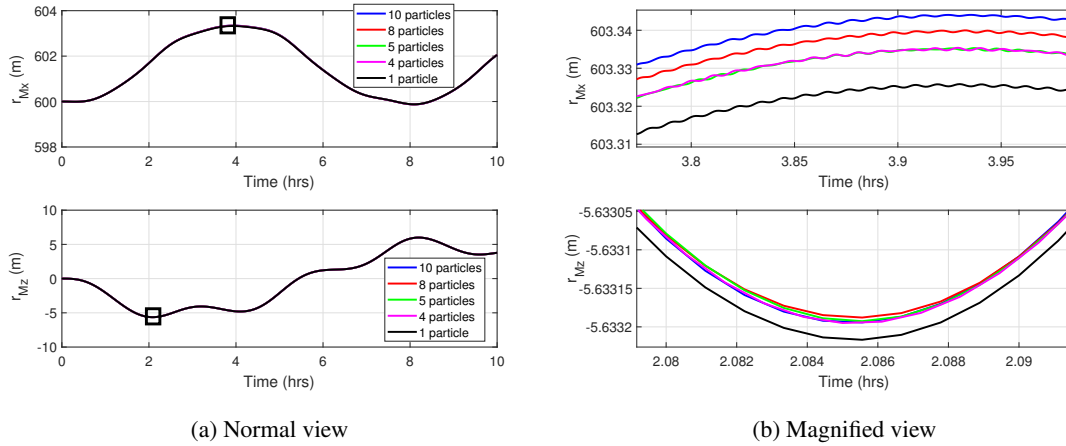(a) Normal view                    (b) Magnified view

Figure 11: The position profiles of the collected mass as the number of particles in the tether model varies.

# V.    Resonance and Lateral Displacement

Even as the lateral motions of the collected mass and the spacecraft are not controlled, large lateral displacements are not desirable as they can be operationally unsafe or unstable. For an object kept at a distance $d$ from the asteroid mass center in the $\hat{\mathbf{x}}_L$ direction, there are essentially two sources of excitation for the lateral movement. First, when the asteroid rotates, the components of the gravitational force in the $\hat{\mathbf{y}}_L$ and/or $\hat{\mathbf{z}}_L$ directions fluctuate due to shape irregularity, which causes the object to deviate laterally from the $\hat{\mathbf{x}}_L$ axis. Second, the object is also subject to pendular motion where gravity acts as a restoring force for excessive lateral deviation. Both sources of lateral movements contain (quasi-)periodic components. When the pendular motion and the asteroid rotation resonate, the object can experience excessive lateral oscillation. Therefore, when designing a gravity tractor mission, such resonance should be avoided. This applies for GT, EGT, and the tethered EGT.

Figure 12 illustrates the pendular motion in the $\hat{\mathbf{x}}_L$-$\hat{\mathbf{z}}_L$ plane, where the asteroid is assumed to be a uniform sphere, and an object (a GT, EGT, or the collected mass) is controlled longitudinally such that the projection of its position vector from the asteroid mass center along the $\hat{\mathbf{x}}_L$ axis is always $d$. When there is a lateral displacement $z$, the only force in the lateral direction is the gravity component parallel to $\hat{\mathbf{z}}_L$ that acts as a restoring force, shown as $\mathbf{f}_g$ in Fig.
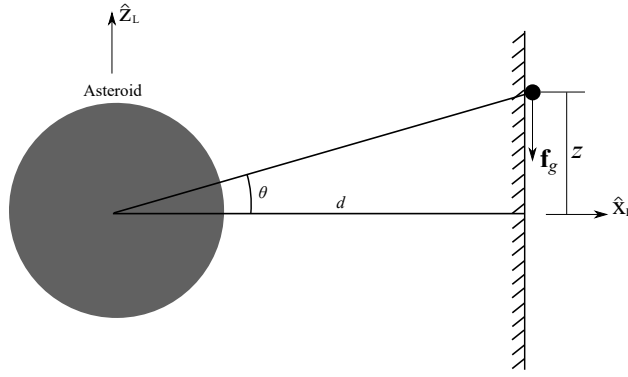
9

Figure 12: Illustration of the pendular motion.

12. The motion of the object in the $\hat{\mathbf{z}}_L$ direction is governed by

$$\ddot{z} = -\frac{\mu_a}{d^2/\cos^2\theta}\sin\theta \tag{5}$$

where $\mu_a$ is the gravitational parameter of the asteroid, and $\theta$ is the angle between $\hat{\mathbf{x}}_L$ and the position vector from the asteroid mass center to the object. Under the assumption of small angle $\theta$, Eq. (5) can be simplified to

$$\ddot{\theta} = -\frac{\mu_a}{d^3}\theta \tag{6}$$

Thus, the period of the pendular motion can be approximated by

$$P \cong 2\pi\sqrt{\frac{d^3}{\mu_a}} \tag{7}$$

Clearly, the period of the pendular motion of an object in the vicinity of an asteroid depends on the distance from the asteroid to the object. Therefore, in order to avoid resonance with the asteroid rotation, some distances should be avoided when designing an EGT mission.

## A. Conventional EGT at an Ellipsoid Performing Simple Spin

The fictitious ellipsoidal asteroid introduced in Sec. IV performs a simple rotation about its smallest diameter, with its spin axis in the same direction as $\hat{\mathbf{y}}_L$. For a conventional EGT placed at at distances 450 m, 500 m, 550 m, or 600 m from the asteroid mass center, the approximate periods of pendular motion are shown in Table 2. For these stations, the amplitudes of lateral oscillation as functions of asteroid rotation period are shown in Fig. 13. It can be seen that the amplitude of lateral oscillation becomes very large in the neighborhood of certain values of the spin period, namely multiples of 1, 2, and 4 of the pendular periods shown in Table 2. The resonance appears to be the strongest when the asteroid rotation period is twice the pendular period, and diminishes as the ratio between the two periods exceeds 4.

Table 2: Approximate periods of pendular motions for an EGT placed at various distances away from a $600 \times 400 \times 300$ m (diameter) ellipsoidal asteroid with density 2000 kg/m$^3$.

| $d$ (m) | 450 | 500 | 550 | 600 |
|---|---|---|---|---|
| Pendular period (hrs) $\approx$ | 7.4 | 8.7 | 10.0 | 11.4 |

## B. Tethered EGT at Itokawa

Itokawa is a slender asteroid that has diameters of approximately 535 m, 294 m, and 209 m, and performs simple rotational motion with a period of 12.1324 hours, with the spin axis having the same direction as $\hat{\mathbf{y}}_L$. Its density is
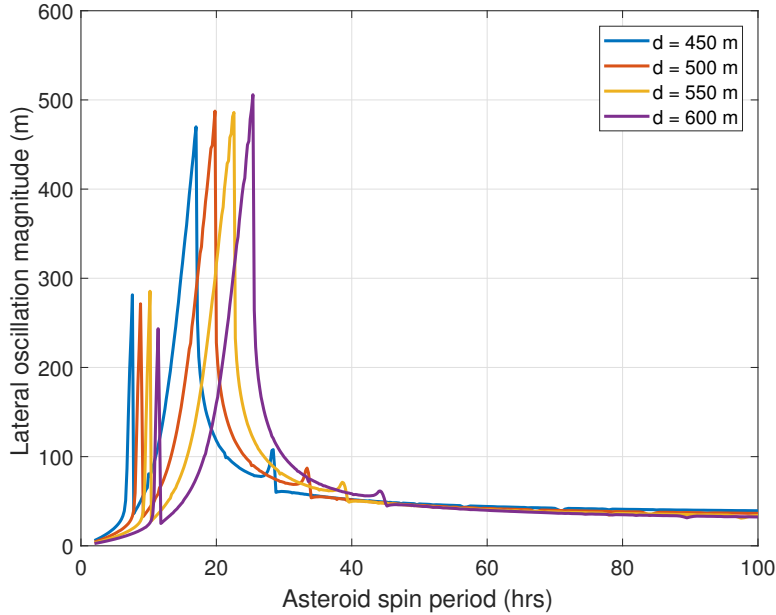
10

Figure 13: Lateral oscillation amplitude of a conventional EGT as a function of asteroid spin period and nominal distance from the asteroid mass center to the EGT.

assumed to be 1955 kg/m$^3$, leading to a gravitational parameter of 2.34 m$^3$/s$^2$. A $20 \times 20$ spherical harmonic model of the asteroid's gravity field is regarded as the true field. The controller is provided with a $3 \times 3$ truncated model as well as a 1% over-estimation. It is assumed that the tether is already deployed, and the tethered EGT is in normal operation. Initially the tether is at its natural length of 3000 m, and unit vectors $\hat{\mathbf{x}}_B$, $\hat{\mathbf{y}}_B$, and $\hat{\mathbf{z}}_B$ have the same directions as $\hat{\mathbf{x}}_L$, $\hat{\mathbf{y}}_L$, and $\hat{\mathbf{z}}_L$, respectively. The control gains are the same as given in Sec. III.

The results for two cases are shown side by side in Figs. 14–16; the nominal distances from the asteroid to the collected mass are 450 m and 500 m. The objective is to demonstrate the effect of resonance on the EGT position and attitude. As is the case in Sec. III in connection with 2008 EV5, after the simulation starts the gravity gradient and the control force keep the tether taut, and the load on the tether remains well within the design capability of the tether throughout the simulation. Figure 14 shows the projections of the position vector from the asteroid mass center to the spacecraft mass center in the directions of $\hat{\mathbf{x}}_L$, $\hat{\mathbf{y}}_L$, and $\hat{\mathbf{z}}_L$. For the case where $d = 450$ m, the amplitude of the longitudinal oscillation is about 10 m, and the amplitude for the lateral oscillation is less than 5 m. There are no anomalies or outliers in the oscillatory motions. When $d = 500$ m, however, clearly the motion of the spacecraft mass center is excited periodically, with peak longitudinal and lateral amplitudes exceeding 20 and 10 meters, respectively. The phenomenon of beating is evident in the projection onto $\hat{\mathbf{z}}_L$.

The projections in the directions of $\hat{\mathbf{x}}_L$, $\hat{\mathbf{y}}_L$, and $\hat{\mathbf{z}}_L$ of the position vector from the asteroid mass center to the collected mass are shown in Fig. 15. When $d = 450$ m, the amplitude of the longitudinal oscillation is about 10 m, and the lateral oscillation has maximum amplitude of about 50 m. The amplitude of the lateral oscillation for the collected mass is greater than that of the spacecraft because the collected mass is much closer to the asteroid, and thus affected more by the irregular gravity field and its variation caused by the asteroid rotation. When $d = 500$ m, the collected mass undergoes oscillations with much greater amplitudes than when $d = 450$ m. In this case, the beating lateral oscillation amplitude can be as high as 300 m, which is greater than the longest semi-diameter of the asteroid.

Similar characteristics are observed in the attitude of the spacecraft; the 3-2-1 Euler angles are shown in Fig. 16. When $d = 450$ m, the spacecraft attitude is well-behaved, with no abnormal excitation, and when $d = 500$ m, it is clear that all three Euler angles are excited periodically. This behavior occurs because the frequency of the forcing function (the asteroid's rotation) is close to the frequency of the pendular motion of the collected mass and the spacecraft. It is clear from the figures that the period of the beating is long compared to the asteroid rotation period. For example, when $d = 500$ m, it takes over 3 days for the first peak amplitude to occur, and the next peak does not show up in over 5 days.
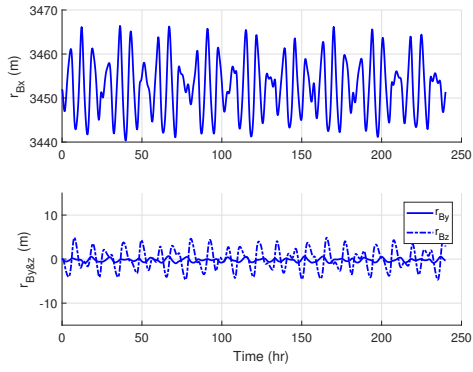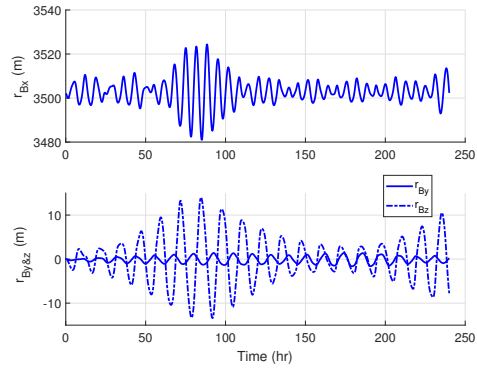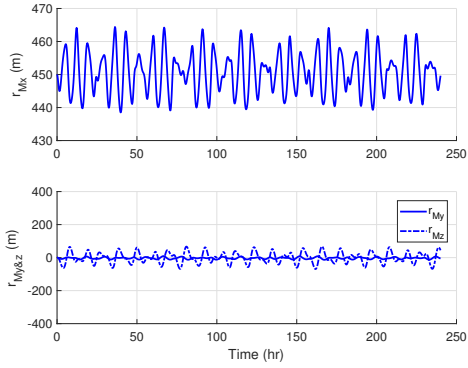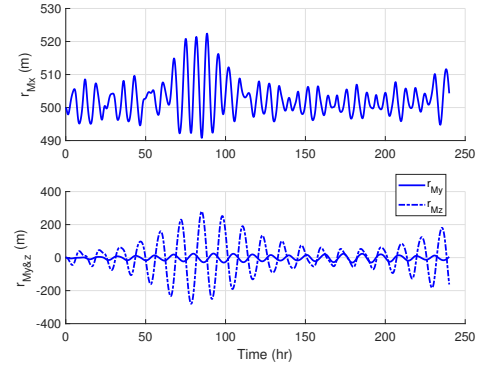
Figure 14: Position of the spacecraft mass center projected onto $\hat{\mathbf{x}}_L, \hat{\mathbf{y}}_L, \hat{\mathbf{z}}_L$ for a tethered EGT operation at Itokawa with 3000-m tether.



Figure 15: Position of the collected asteroidal mass projected onto $\hat{\mathbf{x}}_L, \hat{\mathbf{y}}_L, \hat{\mathbf{z}}_L$ for a tethered EGT operation at Itokawa with 3000-m tether.
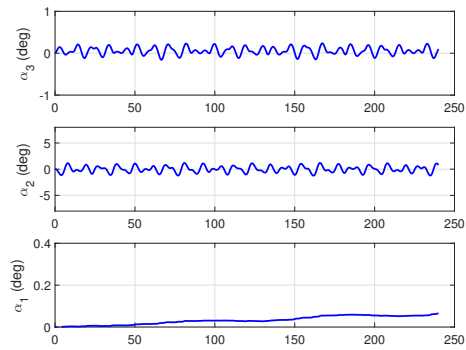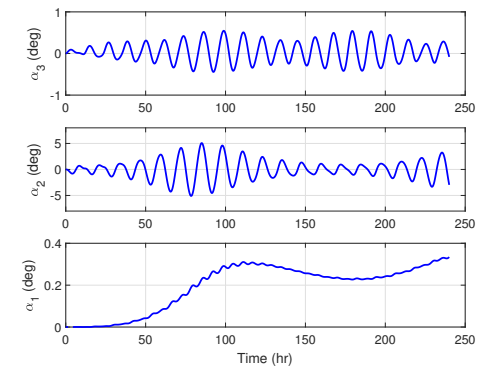


Figure 16: The 3-2-1 Euler Angles for a tethered EGT operation at Itokawa with 3000-m tether.
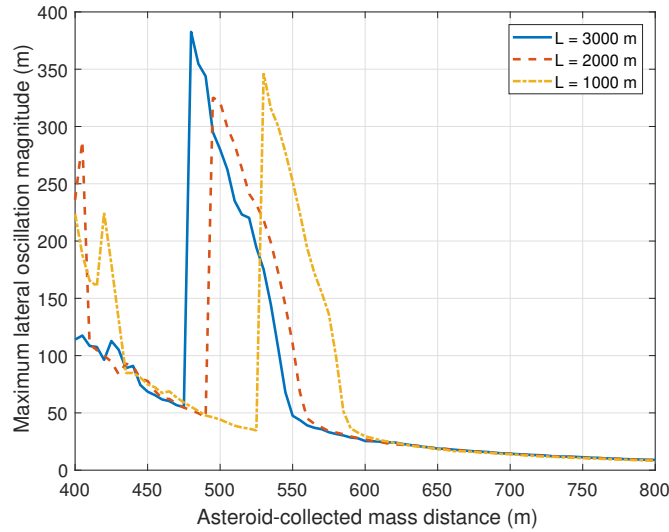
Figure 17: The maximum lateral oscillation amplitude of the collected mass for a tethered EGT at Itokawa as a function of distance between the asteroid and the collected mass, and tether length.

The occurrence of resonance and the ensuing peak oscillation amplitude depend on the length of the tether and the distance between the asteroid and the collected mass. Figure 17 shows the maximum amplitude of lateral oscillation of the collected mass for asteroid-collected mass distance ranging from 400 m to 800 m, and tether lengths of 1000 m, 2000 m, and 3000 m. It can be seen that shortening the tether makes the resonance occur at a greater distance from the asteroid mass center to the collected mass. The curves in Fig. 17 can help mission designers to determine what distances to avoid in designing a tethered EGT operation.
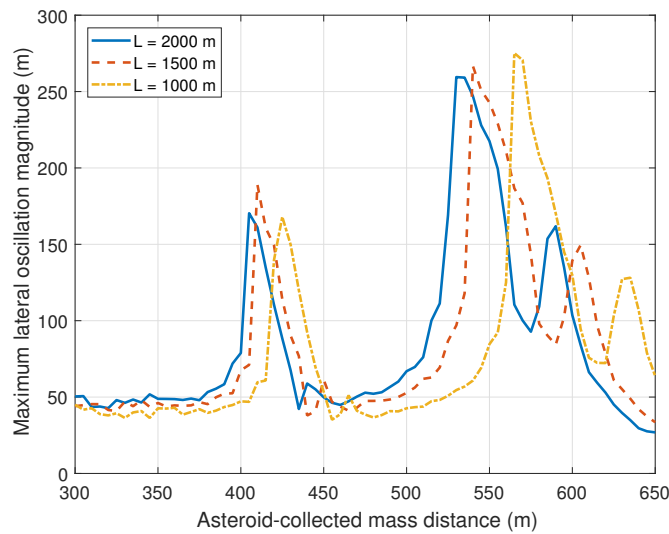


Figure 18: The maximum lateral oscillation amplitude of the collected mass for a tethered EGT at Apophis as a function of distance between the asteroid and the collected mass, and tether length.

## C.   Apophis

Simulations of tethered EGT operations at asteroid Apophis are performed as well. Apophis was discovered in 2004, and it is projected to pass Earth inside the orbits of geosynchronous satellites in 2029. The maximum diameters along the three body axes are approximately 380 m, 270 m, and 230 m. The density is assumed to be 3600 kg/m$^3$, leading to a gravitational parameter 2.66 m$^3$/s$^2$. A $20 \times 20$ spherical harmonic model of the asteroid's gravity field is again regarded as the true field, and the controller is provided with a $3 \times 3$ truncated model as well as a 1% over-estimation. Unlike 2008 EV5 and Itokawa, Apophis does not rotate about only one axis. Instead, it is considered a tumbler, precessing with a period of 27.38 hours, and rotating with a period of 263 hours, as discussed in Ref. [24]. An estimate of attitude for a given epoch is also supplied in Ref. [24].

Simulations performed for Apophis are similar in nature to those conducted for 2008 EV5 and Itokawa; the results obtained for Apophis are similar to those obtained in the case of Itokawa. In particular, the effects of resonance on lateral oscillations are again observed. Note that both Itokawa and Apophis are slender in shape, while 2008 EV5 comes closer to being spherical. Figure 18 shows the maximum amplitudes of lateral oscillation of the collected mass for asteroid-collected mass distance ranging from 300 m to 650 m, and tether lengths of 1000 m, 1500 m, and 2000 m. It can be seen that shortening the tether makes the resonance occur at a greater distance between the asteroid and the collected mass. Depending on the tolerance for uncontrolled lateral deviation, the distances between the asteroid and the collected mass to avoid can be derived from Fig. 18.

# VI.   Conclusions

The dynamics and control of an Enhanced Gravity Tractor (EGT) augmented with a tether for deflecting an asteroid are studied. Use of the tether allows the collected mass to be placed where the EGT would have been without a tether, and the spacecraft to be placed farther away from the asteroid. This improves the fuel efficiency and safety margin of the EGT operation without sacrificing the gravitational attraction between the asteroid and the EGT, provided that the collected mass is significantly more massive than the spacecraft. The tether is modeled as a series of particles connected by spring-dashpot systems. It is shown that a Proportional-Derivative (PD) controller is sufficient to control the spacecraft at the desired position relative to the asteroid, with the assumption that spherical harmonics coefficients of the gravity field of up to the 3$^{\mathrm{rd}}$ degree and order can be estimated to within 1% accuracy. The gravity gradient and the control force keep the tether stretched throughout a normal tethered EGT operation, and the load on the tether is well within the design limit of the tether material. Because the tether is stretched throughout the operation, the number of particles in the tether model has little effect on the mean motion of the spacecraft and the collected mass. That is, the mean motions of the spacecraft and the collected mass can be characterized adequately with one particle in the tether model collocated with the collected mass. It is also shown that the distance from the asteroid mass center to the collected mass cannot be chosen arbitrarily in the case of a rotating slender asteroid. Some distance ranges should be avoided as excessive lateral oscillations can be excited due to resonance between asteroid rotation and pendular motion of the EGT.

# References

[1]   Küppers, M., et al., and the OSIRIS team, "Boulders on Lutetia," *Planetary and Space Science*, Vol. 66, No. 1, 2012, pp. 71–78, Doi:10.1016/j.pss.2011.11.004.

[2]   Veverka, J., et al., "The Landing of the NEAR-Shoemaker Spacecraft on Asteroid 433 Eros," *Nature*, Vol. 413, September 2001, pp. 390–393, Doi:10.1038/35096507.

[3]   Thomas, P. C., Veverka, J., Robinson, M., and Murchie, S., "Shoemaker Crater as the Source of Most Ejecta Blocks on the Asteroid 433 Eros," *Nature*, Vol. 413, September 2001, pp. 394–396, Doi:10.1038/35096513.

[4]   McInnes, C. R., "Deflection of Near-Earth Asteroids by Kinetic Energy Impacts from Retrograde Orbits," *Planetary and Space Science*, Vol. 52, No. 7, 2004, pp. 587–590, Doi: 10.1016/j.pss.2003.12.010.

[5]   Wie, B., "Solar Sailing Kinetic Energy Interceptor Mission for Impacting and Deflecting Near-Earth Asteroids," The 41st AIAA Joint Propulsion Conference and Exhibit, AIAA Paper 2005-3725, Tucson, AZ, July 2005.

[6]   Dachwald, B. and Wie, B., "Solar Sail Kinetic Energy Impactor Trajectory Optimization for an Asteroid-Deflection Mission," *Journal of Spacecraft and Rockets*, Vol. 44, No. 4, 2007, pp. 755–764, Doi: 10.2514/1.22586.

[7] Ahrens, T. J. and Harris, A. W., "Deflection and Fragmentation of Near-Earth Asteroids," *Nature*, Vol. 360, December 1992, pp. 429–433, Doi: 10.1038/360429a0.

[8] Bombardelli, C. and Pelaez, J., "Ion Beam Shepherd for Asteroid Deflection," *Journal of Guidance, Control, and Dynamics*, Vol. 34, No. 4, 2011, pp. 1270–1272, Doi: 10.2514/1.51640.

[9] Lu, E. T. and Love, S. S., "Gravitational Tractor for Towing Asteroids," *Nature*, Vol. 438, Nov. 2005, pp. 177–178, Doi: 10.1038/438177a.

[10] McInnes, C. R., "Near Earth Object Orbit Modification Using Gravitational Coupling," *Journal of Guidance, Control, and Dynamics*, Vol. 30, No. 3, 2007, pp. 870–873, Doi: 10.2514/1.25864.

[11] Wie, B., "Dynamics and Control of Gravity Tractor Spacecraft for Asteroid Deflection," *Journal of Guidance, Control, and Dynamics*, Vol. 31, No. 5, 2008, pp. 1413–1423, Doi: 10.2514/1.32735.

[12] Carroll, J. A., "Ballasted Solar Sail Gravity Tractors for NEO Diversion (or Use)," Planetary Defense Conference, Flagstaff, AZ, April 15–19, 2013. IAA-PDC13-04-02P.

[13] Mazanek, D. D., Merrill, R. G., Belbin, S. P., Reeves, D. M., Earle, K. D., Naasz, B. J., and Abell, P. A., "Asteroid Redirect Robotic Mission: Robotic Boulder Capture Option Overview," AIAA SPACE 2014 Conference and Exposition, Aug. 4–7, 2014, San Diego, CA.

[14] Mazanek, D. D., Reeves, D. M., Hopkins, J. B., Wade, D. W., Tantardini, M., and Shen, H., "Enhanced Gravity Tractor Technique for Planetary Defense," 4th IAA Planetary Defense Conference - PDC 2015, 13–17 April 2015, Frascati, Roma, Italy.

[15] Shen, H. and Roithmayr, C. M., "Towing Asteroids with Gravity Tractors Enhanced by Tethers and Solar Sails," *2015 AIAA/AAS Astrodynamics Specialist Conference, Vail, CO, August 9-13, 2015*.

[16] Cosmo, M. L. and Lorenzini, E. C., Eds., *Tethers in Space Handbook*, 3rd Ed., NASA/CR-97-206807, Smithsonian Astrophysical Observatory, December 1997.

[17] https://www.honeywell-spectra.com/products/fibers/, accessed August 22, 2017.

[18] http://www.dupont.com/content/dam/dupont/products-and-services/fabrics-fibers-and-nonwovens/fibers/documents/Kevlar_Technical_Guide.pdf, accessed August 22, 2017.

[19] Scheeres, D. J. and Schweickart, R. L., "The Mechanics of Moving Asteroids," Planetary Defense Conference: Protecting Earth from Asteroids, Orange County, CA, February 23-26, 2004. AIAA Paper 2004-1446.

[20] Werner, R. A. and Scheeres, D. J., "Exterior Gravitation of a Polyhedron Derived and Compared with Harmonic and Mascon Gravitation Representations of Asteroid 4769 Castalia," *Celestial Mechanics and Dynamical Astronomy*, Vol. 65, No. 3, 1996/1997, pp. 313–344.

[21] https://echo.jpl.nasa.gov/asteroids/shapes/shapes.html, accessed August 22, 2017.

[22] Werner, R. A., "Spherical Harmonics Coefficients for the Potential of a Constant-Density Polyhedron," *Computers & Geosciences*, Vol. 23, No. 10, 1997, pp. 1071–1077.

[23] Scheeres, D. J., *Orbital Motion in Strongly Perturbed Environments: Applications to Asteroid, Comet, and Planetary Satellite Orbiters*, Springer, Heidelberg, 2012.

[24] Pravec, P., et al., "The Tumbling Spin State of (99942) Apophis," Vol. 233, 2014, pp. 48–60.